# AUTOMATED BLOOD VESSEL SEGMENTATION BASED ON DE-NOISING AUTO-ENCODER AND NEURAL NETWORK

**ZHUN FAN[1],[2], JIA-JIE MO[2]**

[1]Guangdong Key Laboratory of Digital Signal and Image Processing, Shantou University, Shantou 515063, China
[2]Department of Electronic Engineering, Shantou University, Shantou 515063, China
E-MAIL: zfan@stu.edu.cn, 12jjmo@stu.edu.cn

**Abstract:**

**Retinal vessel segmentation has been widely used for screening, diagnosis and treatment of cardiovascular and ophthalmologic diseases. In this paper, we propose an automated approach for vessel segmentation in digital retinal images based on de-noising auto-encoders layer-wise initialized neural networks. The proposed method utilized a deep neural network, which is layer-wise initialized by de-noising auto-encoders and fine-tuned by BP algorithm, to segment vessel structures in retinal images. The proposed method is very competitive with the state-of-the-art methods. It achieves an average accuracy of 0.9612, 0.9614, 0.6761, sensitivity of 0.7814, 0.7234, 0.9702, and specificity of 0.9788, 0.9799, 0.9702 on 3 public databases DRIVE, STARE, and CHASE_DB1 respectively. The proposed method is promising for automated blood vessel segmentation.**

**Keywords:**

**Vessel segmentation; Retinal images; Neural networks; De-noising auto-encoders**

## 1 Introduction

Retinal vessel segmentation has been widely used by medical community for screening, diagnosis and treatment of cardiovascular and ophthalmologic diseases, such as diabetes, hypertension, arteriosclerosis and chorodial neovascularization [5]. Manual segmentation of retinal blood vessels is a tedious and time-consuming task which also requires training and skill. Besides, as the number of patients with these diseases increases, an automated retinal vessel segmentation algorithm based computer-assisted diagnostic system is appreciated. However, automated retinal vessel segmentation is also a challenging task. Even in the same retinal image, the shape, thickness and intensity level of retinal vessels may vary hugely in different local areas, due to illumination and deformation of the retinal image. And the centerline reflex, different vessel crossing and branching pattern makes the segment task more challenging.

Many retinal vessel segmentation algorithms have been introduced in the past decades. According whether these algorithms utilized machine learning technique, they can be divided into 2 categories:

Image processing approaches: (1) vessel tracking / tracing [3], (2) matched filtering [1], (3) mathematical morphology [5]. These methods are designed by intuition or personal experience.

Machine learning approaches: Methods utilized machine learning technique are data-drive approaches. Many of them utilize extracted feature vectors to train a classifier to determine whether a pixel from retinal image is belong to vessel or not. For example, Marin $et\ al.$ designed a intensity level and moment invariants-based feature vector to train support vector machines (SVM) for vessel segmentation [9]. Li $et\ al.$ utilized a de-noising auto-encoder (DAE) as feature extractor and a feed-forward network as a classifier [8]. Cheng $et\ al.$ used context-aware hybrid features to train random forests for vessel segmentation [2]. The performance of these methods are mainly determined by 2 factors: feature representation and the classifier.

In this paper, we propose an automated method based on DAEs layer-wise initialized neural networks for retinal vessel segmentation. This method using sliding window to extract patches from retinal image. After reshape them into 1-dimension feature vectors, we utilized DAEs layer-wise initialized neural networks to learn the mapping function from retinal image patches to vessel map patches. At last, reconstruct the prediction vectors to vessel maps. The inspiration of the proposed method comes from [8] and [6], where Li $et\ al.$ proposed a supervised training strategy for DAE, and Hinton $et\ al.$ provided a layer-wise initialization strategy.

The proposed method has been evaluated on 3 different publicly available databases. The average results show that the proposed method is a robust tool for vessel segmentation. The experimental results also demonstrate that the proposed method is very competitive with the stage-of-the-art methods.

The rest of the paper is organized as follows: Section 2 introduce the databases used in this paper. Section 3 explains and illustrates the proposed method. Section 4 shows the experimental results obtained using three public databases, and comparisons with other methods from the literatures. At last, conclusions are provided in Section 5.

## 2 Public Databases

In order to evaluate the vessel segmentation methodology, we conduct our experiment on 3 publicly available databases of retinal images, the DRIVE [14], STARE [7], and CHASE_DB1 [12] databases. These databases have been widely used by other researchers to test their vessel segmentation algorithms because these databases provide manual segmentations or ground truth for performance evaluation.

The DRIVE database contains 40 color retinal images with size of $656 \times 584$ pixels per image. And it is divided into training set and test set. Each of them contains 20 different retinal images. And feild of view (FOV) masks of manual segmenta-

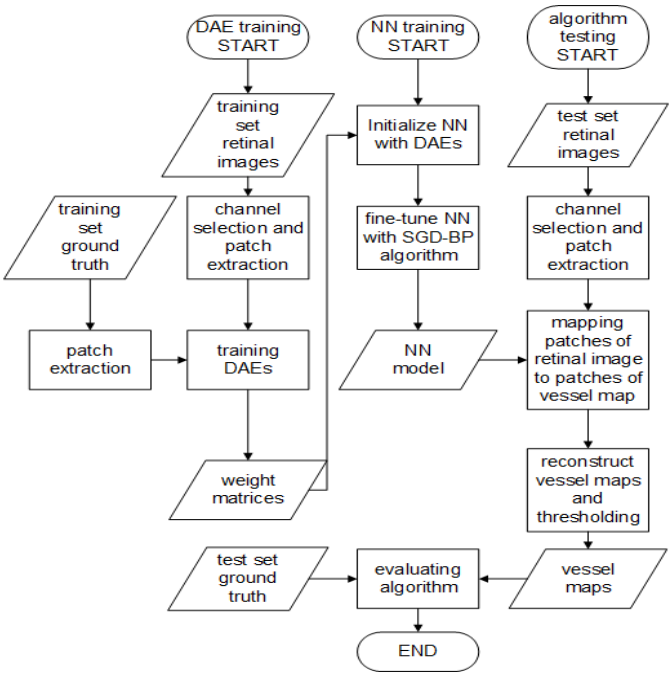


**FIGURE 1.** Overall architecture of the proposed method

(a) (b) (c)

**FIGURE 2.** (a) red channel of RGB retinal image. (b) green channel of RGB retinal image. (c) blue channel of RGB retinal image.

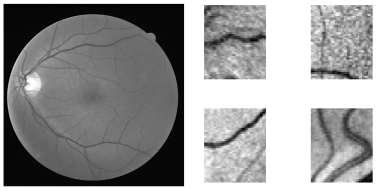

(a) (b)

**FIGURE 3.** (a) G channel of retinal image. (b) 4 patches centralized on different pixels in (a).

tions for the corresponding images are provided in both sets. In practice, researchers usually utilized the training set in algorithm designing and test set in algorithm evaluation.

The STARE database contains 20 color retinal images with size of $700 \times 605$ pixels per image. The FOV masks of manual segmentations for the corresponding images are also provided for all 20 images in STARE. The CHASE_DB1 database contains 28 color retinal images with size of $999 \times 960$ pixels per image. The FOV masks of manual segmentations for the corresponding images are also provided for all 28 images in CHASE_DB1. But both of these databases are not divided into training set and test set. In practice, researchers usually utilized the 'leave-one-out' strategy to design and evaluate algorithms. Which means each test on one single retinal image, is conducted while using the other images to train the learning algorithm.

## 3 Proposed Method

### 3.1 Method Overview

In this paper, we propose a supervised approach based on DAEs layer-wise initialized neural networks for retinal vessel segmentation. The proposed method mainly consists of the following process stages: (1)Utilizing sliding window to pixel-wise extract patches from both retinal images and ground truths from training sets. (2) Training DAEs and use them to initialize the neural network (3) Using stochastic gradient descent based back propagation algorithm with regularization to fine-tune the neural network. (4) Reconstructing the vessel map from the output patches of neural network with a optimized threshold. (5) Comparing the vessel maps to the corresponding ground truths to evaluate the proposed method. The architecture of these process is summarized in FIGURE 1.

### 3.2 Channel Selection and Patch Extraction

#### 3.2.1 Channel Selection

The retinal images from publicly available databases are color images, which contains RGB channels 2. In order to reduce the calculation, we selected only the green channel as the input of learning algorithm. The green channel provides the best vessel-background contrast of the RGB-representation, while the red channel is the brightest color channel and has low contrast, and the blue one offers poor dynamic range. Thus, blood containing elements in the retinal layer, such as vessels, are best represented and reach higher contrast in the green channel [15].

#### 3.2.2 Patch Extraction

In this process step, we use a sliding window with constant size $P$ to extract patches in the G channel of retinal images. Specifically, there are $R \times C$ windows centralized on each pixel in a image with size $R \times C$, respectively. And the values of patches are the same as the pixels of adjacent region under the corresponding window as shown in FIGURE 3. Then reshape these patches into one-dimension vectors with size of $1 \times P^2$, and use them as feature vectors $x$ of each pixel in retinal image. After we produce the label vectors $y$ by conducting the same patch extraction process on the corresponding ground truth, the vessel segmentation task remains as finding the mapping function $\hat{y} = f(x)$ via learning algorithm, where $W$ are the trainable parameter matrices or weight matrices of the learning algorithm.

After channel selection and patch extraction, a training set database contains $S$ retinal images and its corresponding ground truths can be represented by example matrix $\{(x^{(k)}, y^{(k)})\}_{k=1}^{m}, x^{(k)} \in \mathbb{R}^{P^2}, y^{(k)} \in \mathbb{R}^{P^2}$, where $m = R \times C \times S$ and $(x^{(k)}, y^{(k)})$ is the $kth$ patch vectors in the example matrix.

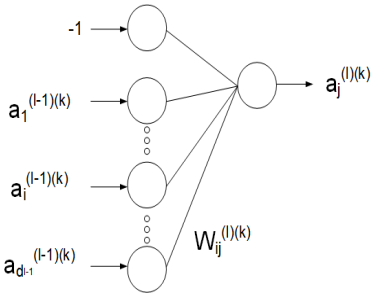


**FIGURE 4.** M-P neuron model.

## 3.3 Artificial Neural Network

### 3.3.1 Neuron Model

In this paper, we utilized the M-P neuron model [13] with $sigmoid$ activation [17] as the basic unit of the neural network. For example, in FIGURE 4, the $jth$ neuron in the $lth$ layer, which connects with the bias neuron and other $d_{l-1}$ neurons with the $kth$ input in previous layer, outputs an activation $a_j^{(l)(k)}$ as follow:

$$\begin{aligned} a_j^{(l)(k)} &= sigmoid(\sum_{i=0}^{d_{l-1}} W_{ij}^{(l)(k)} a_i^{(l-1)(k)}) \\ &= \frac{1}{1+e^{-(\sum_{i=0}^{d_{l-1}} W_{ij}^{(l)(k)} a_i^{(l-1)(k)})}} \end{aligned} \tag{1}$$

### 3.3.2 Network Architecture

In order to learn the complex mapping function, we utilized a 5 layer neural network shown as FIGURE 5. Each neuron in a layer have full-connection with the neuron in the previous layer. We use $W_{ij}^{(l)}$ to denote the weight on the connection between $ith$ neuron in $(l-1)th$ layer and $jth$ neuron in $l$ layer, and $d_i, i = 1, 2, 3.$ to denote the number of neurons in the $ith$ hidden layer.

Each hidden layer serves as a feature extractor. They have the capability to abstract features from low-level intensity information to high-level abstracted feature representations[17]. Since the neural network was designed to predict labels of each components of a $1 \times P^2$ sized patch vector $x$, the number of neurons in both input and output layer are fixed to $P^2$. And notice that the activation function of those neurons are not $softmax$ function, which is wildly used in multi-class classification, but $P^2$ independent $sigmoid$ functions[1].

### 3.3.3 DAEs-based Layer-wise Initialization

De-noising auto-encoders or DAEs, are wildly used as a building block for deep neural networks. In practice, researchers commonly use neural networks with single hidden layer that trained for reconstructing the input $x$ from a corrupted version of the input $x_{noised}$, by using training examples like $\{(x^{(k)}, x_{noised}^{(k)})\}$ with BP Algorithm (Algorithm 1), which will be discussed in details in Section 3.3.4.

[1] $Softmax$ function is the generalized version of $sigmoid$ function, which defined as: $softmax(x)_j = \frac{e^{x_j}}{\sum_{k=1}^{K} e^{x_k}}$

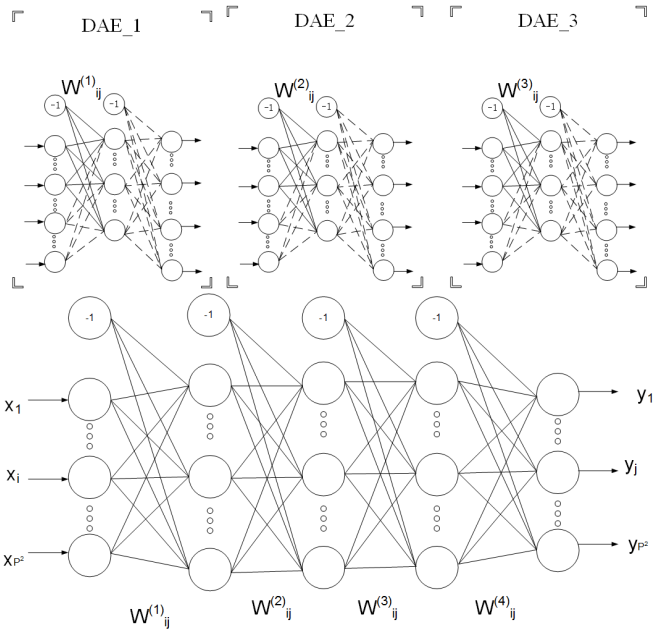


**FIGURE 5.** Architecture of DAEs and neural network.

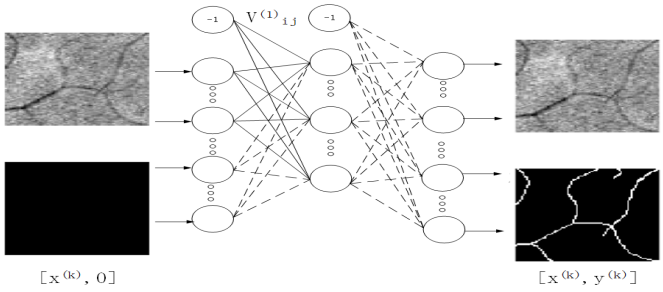


**FIGURE 6.** DAE model, and $V_{ij}^1$ are weights on solid lines.

In this paper, we utilized the supervised training strategy from Li $et\ al.$[8] to train each one of DAEs. Then use the weights between input and hidden layer of one DAE to initialize the corresponding weights in neural network layer by layer.

This supervised training strategy used modified joint examples $\{(x_{mod}^{(k)}, y_{mod}^{(k)})\} = \{([x^{(k)}, 0s], [x^{(k)}, y^{(k)}])\}$ as training examples.

In this case, by applying BP Algorithm, the neurons that connects $x^{(k)}$ in $x_{mod}^k$ with $y^{(k)}$ in $y_{mod}^{(k)}$ will be forced to produce abstracted feature representation that maps $x^{(k)}$ to $y^{(k)}$.

For example, in FIGURE 6, we used the extracted feature vectors and its corresponding ground truth vectors as unmodified training examples $\{(x^{(k)}, y^{(k)})\}$ to train the DAE, and use the first half weights $V_{ij}^1$ (shown as solid lines in FIGURE 6) for initialize the weights $W_{ij}^1$ between the input layer and first hidden layer of neural network in FIGURE 5.

In FIGURE 5, after a hidden layer in neural network been initialized, we can use the activation of the hidden layer of the previous DAE as unmodified $x^{(k)}$ to go though the same process for training the next DAE, until we have enough weights matrices to initialize all the weights in neural network.

For example, the weights learned by DAE and used to initialize the first hidden layer of neural network, can be visualized

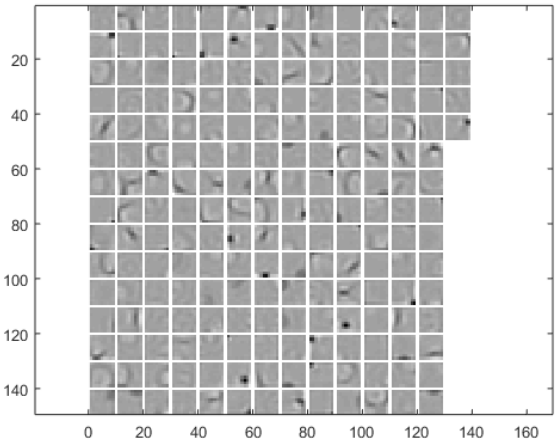


**FIGURE 7.** weights learned by 200 DAE neurons.

as FIGURE 7.

#### 3.3.4 Fine-tuning Neural Network

The process of training neural network is a process of finding the best weight matrices. In order to quantifying the effectiveness of the weight matrices, we define the loss function $L(W_{ij}^{(l)})$ as follows:

$$L(W_{ij}^{(l)}) = E(W_{ij}^{(l)}) + \Psi(W_{ij}^{(l)})$$
$$= \frac{1}{2m}\sum_{k=1}^{m}\sum_{j=1}^{p^2}(\hat{y}_j^{(k)} - y_j^{(k)})^2 + \frac{\lambda}{2}\sum_{l}\sum_{i}\sum_{j}(W_{ij}^{(l)})^2 \quad (2)$$

where $E(W_{ij}^{(l)})$ is the accumulated mean square error over $m$ examples, $\Psi(W_{ij}^{(l)})$ is the regularization term, and $\lambda$ is a punitive parameter for the regularization term.

While we training the neural network, or $\min_{W_{ij}^{(l)}} L(W_{ij}^{(l)})$ from the perspective of minimizing the loss Function (2), the regularization term prevents weights from getting too big. If the weights keep in small values, the architecture of neural network is relatively simple, in which case prevents over-fitting[2].

The most commonly used method for minimizing the loss function in practice, is stochastic gradient descent (SGD) based accumulated error back propagation (BP) algorithm with regularization[17].

The basic idea of SGD is simple. Firstly, randomly divide the training set into subsets or batches with $m$ examples. In each training epoch, using gradient $\frac{\partial L(W_{ij}^{(l)})}{\partial W_{ij}^{(l)}}$ over one batch to determine whether increase or decrease each $W_{ij}^{(l)}$ for minimizing the loss Function (2). Then update all $W_{ij}^{(l)}$ simultaneously with the following rule:

$$W_{ij}^{(l)} \leftarrow W_{ij}^{(l)} - \frac{\eta}{m}\sum_{k=1}^{m}\frac{\partial L(W_{ij}^{(l)})}{\partial W_{ij}^{(l)}} = W_{ij}^{(l)} + \triangle(W_{ij}^{(l)}) \quad (3)$$

[2]It's natural to consider those links with 0 weights are disconnected. The smaller weight a link has, the less influence it can provide to the neurons in the next layer, in which case, the architecture of neural network is less complex.

**Algorithm 1** SGD based BP algorithm with regularization

**Input:** training set $\mathbf{D} = \{(x^{(k)}, y^{(k)})\}_{k=1}^{m\times B}$, learning rate $\eta$
Initialize all $W_{ij}^{(l)}$.
Reset the number of epoch: $epoch \leftarrow 0$
**repeat**
  Randomly divide $\mathbf{D}$ into $\mathbf{B} = \{(batch_b)\}_{b=1}^{B}$.
  **for** $b = 1$ **to** $B$ **do**
    Compute $a_i^{(l)(k)}$ of all neurons with Function (1).
    Compute $\triangle(W_{ij}^{(l)})$ of all $W_{ij}^{(l)}$ with Function (4), (5) and (6).
    Update all $W_{ij}^{(l)}$ with Function (3), simultaneously.
  **end for**
  $epoch \leftarrow epoch + 1$
**until** Reached the maximum number of epoch

where $\eta$ is the given learning rate.

In order to compute all $\triangle(W_{ij}^{(l)})$ iteratively, back propagation algorithm use chain rule to calculate gradients by propagating loss following the back-direction[3].

Specifically, each $\triangle(W_{ij}^{(l)})$ is calculate as follow:

$$\triangle(W_{ij}^{(l)}) = \frac{\eta}{m}\sum_{k=1}^{m} a_i^{(l)(k)} t_j^{(l)(k)} - \frac{\eta\lambda}{m}W_{ij}^{(l)} \quad (4)$$

where $k$ indicates the neural network tasks the $kth$ example as input.

The activation term $a_i^{(l)(k)}$ can be calculated with Function (1).

The iterative term $t_j^{(l)(k)}$ can be calculated iteratively as follow:

$$t_j^{(l)(k)} = a_j^{(l+1)(k)}(1 - a_j^{(l+1)(k)})\sum_{i=0}^{d_{l+2}} W_{ji}^{(l+1)} t_i^{(l+1)(k)} \quad (5)$$

where $l \in \mathbb{N}$ & $l \leq l_{max} - 2$.
The iteration ends with:

$$t_j^{(l_{max}-1)(k)} = \hat{y}_j^{(k)}(1 - \hat{y}_j^{(k)})(y_j^{(k)} - \hat{y}_j^{(k)}) \quad (6)$$

To summarize, the pseudo-code for SGD based BP algorithm with regularization shows as Algorithm 1

### 3.4 Patch Reconstruct and Optimized Thresholding

#### 3.4.1 Patch Reconstruct

After we feed the fine-tuned neural network with feature vectors $x^{(k)}$, the output of neural network is probability vector $\hat{y}^{(k)}$, in which each component $\hat{y}_j^{(k)}$ of $\hat{y}^{(k)}$ stands for the probability of the pixel corresponding to $x_j^{(k)}$ belong to vessel pixels given $x^{(k)}$.

Because of the application of sliding window with size $P \times P$ for patch extraction in Section 3.2.2, the probability of each pixel in original retinal image can be calculated by averaging all corresponding probability in $P^2$ different patch vectors. With this strategy, we can reconstruct a probability map with the group of patches that belonged to the same retinal image.

[3]The back direction is the direction from output layer to input layer.

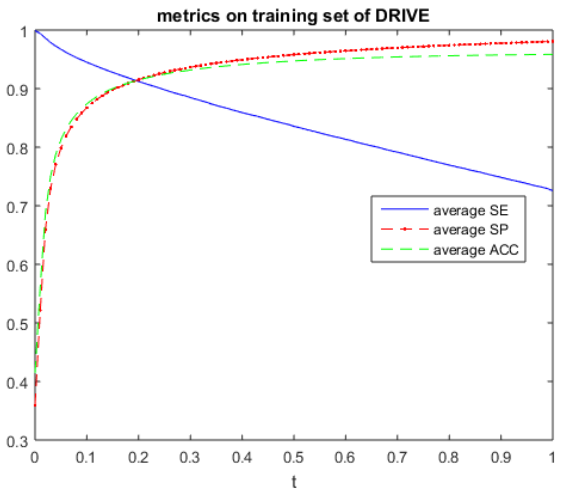


**FIGURE 8.** optimize t by traversal.

### 3.4.2 Optimized Thresholding

In order to evaluate the vessel segment algorithm by comparer with ground truth, the finial result must be a vessel map with binary values. After we obtained the probability map by patch reconstruction, a thresholding process for producing vessel map with binary value is needed. In this paper, given a probability map $p(r, c)$ of size $R \times C$, the corresponding vessel map $v(r, c)$ is computed as follows:

$$v(r,c) = \begin{cases} 0 & \text{if } p(r,c) < threshold(p) = t \times \mathbf{Otsu}(p) \\ 1 & otherwise \end{cases} \tag{7}$$

where $\mathbf{Otsu}(p)$ is the threshold computed by **Otsu** method [18], and $t$ is a constant selected by searching over a limited discrete parameter space. For example, while we choosing a constant $t$ on DRIVE database, we calculated the average evaluation metrics(SE (8), SP (9), ACC (10), shows as FIGURE 8.

As FIGURE 8 shows, as $t$ increases, the average SE (8) drops sharply, and both SP (9) and ACC (10) increase. For the sake of vessel segmentation performance, we set $t$ to a value, which its corresponding SP (9) is near 0.97 on training set. And we utilized the same $t$ to perform thresholding on the test set.

## 4 EXPERIMENTAL RESULTS

### 4.1 Evaluation Criterion

In retinal vessel segmentation, researchers evaluate their methods by comparing the vessel map from algorithm prediction with the corresponding ground truth. Therefore, we can divide the pixels in the vessel map into true positive (TP), false positive (FP), negative (FN) and true negative (TN) by comparing them with the corresponding ground truth labels. And their definitions are list in the TABLE 1.

While the pixels in vessel map been categorized, we can use these metrics to compare the performance of the proposed method with other state-of-the-art methods: sensitivity (SE), specificity (SP) and accuracy (ACC). They are defined as follows:

**TABLE 1.** Categories of pixels in the algorithm output.

| PIXEL CATEGORIES | VESSEL PIXELS | OTHERS |
|---|---|---|
| PREDICTED AS VESSEL | $TP$ | $FP$ |
| PREDICTED AS OTHERS | $FN$ | $TN$ |

**TABLE 2.** Performance on test set of DRIVE. The 15th is the worst result, and 16th is the best.

| RETINAL IMAGE | SE | SP | ACC |
|---|---|---|---|
| 1 | 0.856 | 0.9745 | 0.964 |
| 2 | 0.8219 | 0.9816 | 0.9652 |
| 3 | 0.7617 | 0.9782 | 0.9566 |
| 4 | 0.7658 | 0.9841 | 0.9640 |
| 5 | 0.7293 | 0.9876 | 0.9634 |
| 6 | 0.6829 | 0.9895 | 0.9597 |
| 7 | 0.752 | 0.9765 | 0.9560 |
| 8 | 0.7037 | 0.9760 | 0.9526 |
| 9 | 0.6733 | 0.9906 | 0.9649 |
| 10 | 0.7643 | 0.9824 | 0.9644 |
| 11 | 0.7897 | 0.9701 | 0.9540 |
| 12 | 0.7931 | 0.9794 | 0.9633 |
| 13 | 0.7259 | 0.9842 | 0.9589 |
| 14 | 0.8281 | 0.9707 | 0.9592 |
| **15** | **0.8855** | **0.9425** | **0.9385** |
| **16** | **0.7913** | **0.9862** | **0.9686** |
| 17 | 0.7362 | 0.9853 | 0.9643 |
| 18 | 0.8285 | 0.9793 | 0.9673 |
| 19 | 0.8897 | 0.9764 | 0.9692 |
| 20 | 0.8489 | 0.9803 | 0.9707 |
| AVERAGE | 0.7814 | 0.9788 | 0.9612 |

$$SE = TP/(TP + FN) \tag{8}$$

$$SP = TN/(TN + FP) \tag{9}$$

$$ACC = (TP + TN)/(TP + TN + FP + FN) \tag{10}$$

Metrics SE indicates the ratio of vessel pixels correctly predicted to total vessel pixels. Metrics SP indicates the ratio of none-vessel pixels correctly predicted to total none-vessel pixels. And metrics ACC is a global measure providing the ratio of pixels correctly predicted to all pixels.

### 4.2 Performance in detail on DRIVE

The performance of proposed method on each retinal images in test set of DRIVE database is listed in TABLE 2. The proposed method achieved an average SE of 0.7814, SP of 0.9788 and ACC of 0.9612, on 20 different retinal images of DRIVE. We consider the vessel segment result of 15th image, which has the lowest ACC, as the worst result, while 16th is the best.

In the case of the 15th image, the retinal image, ground truth, vessel map are shown in FIGURE 9. In the 15th entry of TABLE 2, SE of 0.8855 indicates the algorithm picks up $88.55\%$ of vessel, and SP of 0.9425 indicates the algorithm failed to predict $5.75\%$ of background, which is way too much. And these statistics reflected in the algorithm output in FIGURE 9.

In the case of the 16th image, the retinal image, ground truth, vessel map are shown in FIGURE 10.

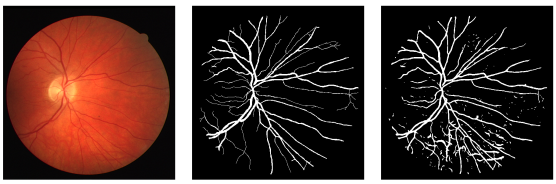

(a) (b) (c)

**FIGURE 9.** (a) 15th retinal image in test set of DRIVE. (b) corresponding ground truth. (c) algorithm output.

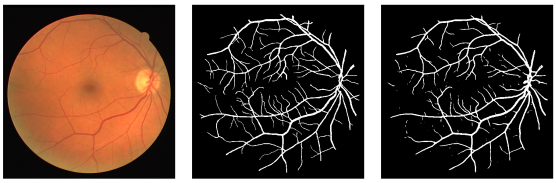

(a) (b) (c)

**FIGURE 10.** (a) 16th retinal image in test set of DRIVE. (b) corresponding ground truth. (c) algorithm output.

### 4.3 Comparison to Other Methods

In order to emphasize the effectiveness of the proposed method, we compare its performance with other existing state-of-the-art vessel segmentation methods on three most popular public databases: the DRIVE database, the STARE database and the CHASE_DB1 database. TABLE 3, TABLE 4 and TABLE 5 shows the average performance of the proposed method and the others in three databases, respectively.

The average results show that the proposed method is a robust tool for vessel segmentation. The comparison also demonstrate that the proposed method is very competitive with the stage-of-the-art methods.

## 5 CONCLUSION

In this paper, we propose a new supervised retinal blood vessel segmentation method, which is based on DAEs layer-wise initialized neural network. The results(SE of 0.7814, SP of 0.9788 and ACC of 0.9612 on DRIVE, SE of 0.7834, SP of 0.9799 and ACC of 0.9654 on STARE, SE of 0.7661, SP of 0.9704 and ACC of 0.9573 on CHASE_DB1) manifest that our method is effective and robust for vessel segmentation in retinal images.

**TABLE 3.** Comparison of vessel segmentation methods on DRIVE.

| METHODS | YEAR | SE | SP | ACC |
|---|---|---|---|---|
| PROPOSED METHOD | 2016 | 0.7814 | 0.9788 | 0.9612 |
| LI *et al.*[8] | 2015 | 0.7569 | 0.9816 | 0.9527 |
| AZZOPARDI *et al.*[1] | 2015 | 0.7655 | 0.9704 | 0.9442 |
| FRAZ *et al.*[4] | 2012 | 0.7655 | 0.9704 | 0.9442 |
| FRAZ *et al.*[5] | 2012 | 0.7406 | 0.9807 | 0.9480 |
| CHENG *et al.*[2] | 2014 | 0.7252 | 0.9798 | 0.9474 |
| MARIN *et al.*[9] | 2011 | 0.7067 | 0.9807 | 0.9441 |
| MIRI *et al.*[11] | 2011 | 0.7352 | 0.9795 | 0.9430 |
| MENDONCA *et al.*[10] | 2006 | 0.7344 | 0.9764 | 0.9452 |
| YOU *et al.*[16] | 2011 | 0.7410 | 0.9751 | 0.9434 |

**TABLE 4.** Comparison of vessel segmentation methods on STARE.

| METHODS | YEAR | SE | SP | ACC |
|---|---|---|---|---|
| PROPOSED METHOD | 2016 | 0.7834 | 0.9799 | 0.9654 |
| LI *et al.*[8] | 2015 | 0.7726 | 0.9844 | 0.9628 |
| AZZOPARDI *et al.*[1] | 2015 | 0.7716 | 0.9701 | 0.9563 |
| FRAZ *et al.*[4] | 2012 | 0.7311 | 0.9680 | 0.9442 |
| FRAZ *et al.*[5] | 2012 | 0.7548 | 0.9763 | 0.9534 |
| MENDONCA *et al.*[10] | 2006 | 0.6996 | 0.9730 | 0.9440 |
| YOU *et al.*[16] | 2011 | 0.7260 | 0.9756 | 0.9497 |

**TABLE 5.** Comparison of vessel segmentation methods on CHASE_DB1.

| METHODS | YEAR | SE | SP | ACC |
|---|---|---|---|---|
| PROPOSED METHOD | 2016 | 0.7656 | 0.9704 | 0.9573 |
| LI *et al.*[8] | 2015 | 0.7507 | 0.9793 | 0.9581 |
| AZZOPARDI *et al.*[1] | 2015 | 0.7585 | 0.9587 | 0.9387 |
| FRAZ *et al.*[5] | 2012 | 0.7224 | 0.9711 | 0.9469 |


## Acknowledgements

This research work was supported by Guangdong Key Laboratory of Digital Signal and Image Processing, the National Natural Science Foundation of China under Grant (61175073, 61300159, 61332002, 51375287, 61370102, 61170193), Jiangsu Natural Science Foundation (BK20130808). Innovative Application and Integrated Services Platform of the First Generation of Numerical Control in the Eastern Part of Guangdong Province, support no. (2013B011304002).


## References


[1] George Azzopardi, Nicola Strisciuglio, Mario Vento, and Nicolai Petkov. Trainable cosfire filters for vessel delineation with application to retinal images. *Medical Image Analysis*, 19(1):46–57, 2015.

[2] Erkang Cheng, Liang Du, Yi Wu, Ying J. Zhu, Vasileios Megalooikonomou, and Haibin Ling. Discriminative vessel segmentation in retinal images by fusing context-aware hybrid features. *Machine Vision and Applications*, 25(7):1779–1792, 2014.

[3] Konstantinos K. Delibasis, Aristides I. Kechriniotis, C. Tsonos, and Nicholas Assimakis. Automatic model-based tracing algorithm for vessel segmentation and diameter estimation. *Computer Methods and Programs in Biomedicine*, 100(2):108–122, 2010.

[4] M. M. Fraz, S. A. Barman, P. Remagnino, A. Hoppe, A. Basit, B. Uyyanonvara, A. R. Rudnicka, and C. G. Owen. An approach to localize the retinal blood vessels using bit planes and centerline detection. *Computer Methods and Programs in Biomedicine*, 108(2):600–616, 2012.

[5] M. M. Fraz, P. Remagnino, A. Hoppe, B. Uyyanonvara, A. R. Rudnicka, C. G. Owen, and S. A. Barman. Blood vessel segmentation methodologies in retinal images–a survey. *Comput Methods Programs Biomed*, 108(1):407–33, 2012.

[6] Geoffrey E. Hinton, Simon Osindero, and Yee-Whye Teh. A fast learning algorithm for deep belief nets. *Neural Computation*, 18(7):1527–1554, 2006.

[7] A. D. Hoover, V. Kouznetsova, and M. Goldbaum. Locating blood vessels in retinal images by piecewise threshold probing of a matched filter response. *IEEE Transactions on Medical Imaging*, 19(3):203–210, 2000.

[8] Q. Li, B. Feng, L. Xie, P. Liang, H. Zhang, and T. Wang. A cross-modality learning approach for vessel segmentation in retinal images. *IEEE Trans Med Imaging*, 2015.

[9] Diego Marin, Arturo Aquino, Manuel Emilio Gegundez-Arias, and Jose Manuel Bravo. A new supervised method for blood vessel segmentation in retinal images by using gray-level and moment invariants-based features. *Ieee Transactions on Medical Imaging*, 30(1):146–158, 2011.

[10] Ana Maria Mendonca, Aurelio Campilho, and A. Segmentation of retinal blood vessels by combining the detection of centerlines and morphological reconstruction. *Ieee Transactions on Medical Imaging*, 25(9):1200–1213, 2006.

[11] Mohammad Saleh Miri, Ali Mahloojifar, and A. Retinal image analysis using curvelet transform and multistructure elements morphology by reconstruction. *Ieee Transactions on Biomedical Engineering*, 58(5):1183–1192, 2011.

[12] C. G. Owen, A. R. Rudnicka, R Mullen, S. A. Barman, D Monekosso, P. H. Whincup, J Ng, and C Paterson. Measuring retinal vessel tortuosity in 10-year-old children: validation of the computer-assisted image analysis of the retina (caiar) program. *Investigative Ophthalmology and Visual Science*, 50(5):2004–10, 2009.

[13] G. Piccinini. The first computational theory of mind and brain: A close look at mcculloch and pitts's "logical calculus of ideas immanent in nervous activity". *Synthese*, 141(2):175–215, 2004.

[14] J.J. Staal, M.D. Abramoff, M. Niemeijer, M.A. Viergever, and B. van Ginneken. Ridge based vessel segmentation in color images of the retina. *IEEE Transactions on Medical Imaging*, 23(4):501–509, 2004.

[15] Thomas Walter, Pascale Massin, Ali Erginay, Richard Ordonez, Clotilde Jeulin, and Jean-Claude Klein. Automatic detection of microaneurysms in color fundus images. *Medical Image Analysis*, 11(6):555–566, 2007.

[16] Xinge You, Qinmu Peng, Yuan Yuan, Yiu-ming Cheung, and Jiajia Lei. Segmentation of retinal blood vessels using the radial projection and semi-supervised approach. *Pattern Recognition*, 44(10-11):2314–2324, 2011.

[17] Zhou Zhihua. *Machine Learning*. Tsinghua University Press, Beijing, 2015.

[18] N. Zhu, G. Wang, G. Yang, and W. Dai. A fast 2d otsu thresholding algorithm based on improved histogram. In *Pattern Recognition, 2009. CCPR 2009. Chinese Conference on*, pages 1–5, Nov 2009.